

β -Si₃N₄(0001)/Si(111) interface: Phosphorus defects, valence band offsets, and their role of passivating the interface states

E. Flage-Larsen* and O. M. Løvvik

SINTEF Materials and Chemistry, P.O. Box 124 Blindern, Forskningsveien 1, N-0314 Oslo, Norway

C. M. Fang and G. Kresse

Faculty of Physics and Center for Computational Materials Science, University of Vienna, Sensengasse 8/12, A-1090 Vienna, Austria

(Received 31 May 2013; published 18 October 2013)

This work investigates the β -Si₃N₄(0001)/Si(111) interface based on a model with fully saturated interface bonds. The charge transfer at the interface and band alignment are calculated. The band alignment is corrected by GW_0 calculations. Furthermore, we investigate how substitutional phosphorus defects affect the electronic structure of the interface, in particular how they saturate the interface states and modify the valence band offsets.

DOI: [10.1103/PhysRevB.88.165310](https://doi.org/10.1103/PhysRevB.88.165310)

PACS number(s): 73.20.Hb, 88.40.jj, 31.15.E-

I. INTRODUCTION

Bulk silicon-nitride compounds have traditionally been used due to their sterling wear resistance and temperature toughness.¹ However, silicon nitride also exhibits excellent passivation properties^{1,2} and the semiconductor industry has employed silicon nitride as an alternative to, for instance, silicon oxide due to better dielectric and antireflective properties. Amorphous silicon nitride can be efficiently grown on silicon by means of nitridation, for example, through the use of NH₃ with low cost and controllable thickness. Consequently amorphous silicon nitride is also common on top of industrial grade silicon solar cells.

However, even though silicon nitride is extensively used for passivation on silicon, detailed knowledge of the passivation properties and the microscopic electronic properties of these interfaces is lacking, even for crystalline silicon nitride. For example, it is not well established if and how the band offset between silicon nitride and other materials changes as a function of different defects or how the passivation properties depend on the microscopic structure of defects and interface bonds. Efforts to create thin layers of crystalline silicon nitride on top of crystalline silicon are also still an ongoing experimental challenge. Previous experimental studies of the band offsets between silicon and silicon nitride report scattered values between 1.5 and 1.9 eV.³⁻⁸ The source of this is somewhat unknown, but processing conditions and thus incorporated defects are most likely highly relevant in this context. Few computational studies have investigated the silicon/silicon-nitride interface and calculated the valence band offsets, although, a recent study of Yang *et al.*⁹ reports a valence band offset of 1.52 eV in seemingly good agreement with some of the experiments.

The first model of α - and β -silicon-nitride (0001) on silicon (111) was proposed¹⁰ by Zhao and Bachlechner. They created the interface by maximizing the number of Si-N bonds, which led to an interface that contained unsaturated bonds. Both the α - and β -silicon-nitride were investigated and showed similar charge transfer and electronic structure, which is expected from the similarities of the bulk phases. Recent literature¹¹ concludes that the β phase is the most stable among the silicon-nitride phases.

Early experimental results¹² indicated that the interface bonds of the silicon/silicon-nitride system should be saturated. Yang and coworkers recently suggested⁹ the structure of such a model and showed that it was energetically more stable than the unsaturated model of Zhao and Bachlechner. Yang and coworkers also calculated the valence band offset and claimed this to be in good agreement with the experimental determinations.^{4,6,8,13} Their model is considered to be the currently best fit between the silicon (111) substrate and β -silicon-nitride (0001) with a lattice mismatch of less than 1% and saturated interface bonds.

In this work, we follow the initial study of Yang and coworkers and additionally introduce phosphorus defects and study their electronic structure. Phosphorus is used in industrial solar cells for the emitter to achieve high n -type doping. Its influence on the structural and electronic properties is highly relevant for a full microscopic understanding of the silicon/silicon-nitride interface, since industrial solar cells are usually strongly n -type at the front side, where one aims to avoid electron-hole recombination losses.

II. COMPUTATIONAL DETAILS

The density functional theory (DFT) calculations were based on the Perdew-Burke-Ernzerhof (PBE)¹⁴ exchange-correlation functional and performed using the Vienna Ab-initio Simulation Package (VASP).¹⁵⁻¹⁷ An energy cutoff of 500 eV with a \vec{k} -point sampling of $9 \times 9 \times 3$ was used. All relaxations were terminated when the residual forces were less than 0.005 eV/Å for the interface and 0.001 eV/Å for the bulk calculations. The volume was kept fixed during relaxations of the phosphorus in the interface model. The GW_0 calculations were performed on a $2 \times 2 \times 1$ \vec{k} -point grid with three iterations for the eigenvalues in the Green's function. Convergence in the third iteration is typically better than 5 meV. The orbitals were not updated. This also implies that the interface dipole (related to the charge density of the orbitals) does not change from DFT to the GW_0 calculations. Hence the change of the valence band and conduction band offsets can be determined directly from fast and convenient GW_0 bulk calculations. The corresponding GW_0 valence band

shifts for Si and Si₃N₄ are already documented in Ref. 11. Finally, we note that in previous tests for bulk systems, the GW_0 procedure has yielded very good agreement with fully self-consistent GW calculations.¹¹

Interface energies were calculated as

$$E_i = [E(m\text{Si}/n\text{Si}_3\text{N}_4) - mE(\text{Si}) - nE(\text{Si}_3\text{N}_4)]/2A, \quad (1)$$

where $E(m\text{Si}/n\text{Si}_3\text{N}_4)$ is the energy of the interface model, with m Si units and n Si₃N₄ units, while $E(\text{Si})$ and $E(\text{Si}_3\text{N}_4)$ are the respective bulk energies. The interface area is A (our model always possesses two identical interfaces).

The calculation of the relative total energy differences upon phosphorus substitution was performed with the following energy references

$$\Delta E = E(\text{P@Si/Si}_3\text{N}_4) - E(\text{Si/Si}_3\text{N}_4) - [E(\text{P@Si}) - E(\text{Si})], \quad (2)$$

and

$$\Delta E' = E(\text{P@Si/Si}_3\text{N}_4) - E(\text{Si/Si}_3\text{N}_4) - [E(\text{P@Si/Si}_3\text{N}_4') - E(\text{Si/Si}_3\text{N}_4')], \quad (3)$$

where $E(\text{P@Si/Si}_3\text{N}_4)$, $E(\text{Si/Si}_3\text{N}_4)$, $E(\text{P@Si})$, $E(\text{Si})$, $E(\text{P@Si/Si}_3\text{N}_4')$, and $E(\text{Si/Si}_3\text{N}_4')$ are the energy of the interface model with phosphorus incorporated in a given layer, the interface model, bulk silicon with phosphorus, bulk silicon, the energy of the largest interface model with phosphorus in the bulk silicon part, and the largest interface model without phosphorus, respectively.

Furthermore, the valence band offset was calculated as follows:

$$E_{\text{VBO}} = (E_{\text{VBM}} - E^{\text{ref}})_{\text{Si}} - (E_{\text{VBM}} - E^{\text{ref}})_{\text{Si}_3\text{N}_4} + \Delta E^{\text{ref}}. \quad (4)$$

Here E_{VBM} is the top of the valence band for the bulk Si and Si₃N₄, respectively, evaluated using the respective bulk cells and a very dense k -point sampling to converge E_{VBM} . E^{ref} is a properly chosen reference energy that should converge rapidly with respect to k -points and the number of layers in the interface calculation. Similarly, ΔE^{ref} is the difference in the reference energy between the respective bulk constituents in the interface model ($E_{\text{Si}}^{\text{ref}}$ for Si on the Si side, $E_{\text{Si}_3\text{N}_4}^{\text{ref}}$ for Si on the Si₃N₄ side) and is evaluated as: $\Delta E^{\text{ref}} = (E_{\text{Si}}^{\text{ref}} - E_{\text{Si}_3\text{N}_4}^{\text{ref}})$. As reference energy, different quantities may be chosen; the charge neutrality level, planar averaged electrostatic potentials, or inner atomic core levels of some selected constituent atom. In this work we used the latter approach, where the energy of the silicon 1s states in Si and Si₃N₄ was used to align the valence band maxima.¹⁸

In order to estimate the charge transfer, the electron occupation on each atom was calculated using zero flux partitioning of the electron density (Bader analysis).^{19,20} The core electrons were included and the electron density grid was doubled with respect to the default high accuracy grids to reduce aliasing errors. Visualizations were performed in VESTA.²¹

III. RESULTS AND DISCUSSIONS

A. Comparisons of the two interface models

In order to compare the stability of the two models, the structures based on the recent work by Yang *et al.*⁹ and the earlier work by Zhao and Bachlechner¹⁰ were optimized.

Contrary to the initial study of Yang *et al.*⁹ we did not include a vacuum layer or terminating hydrogen bonds. Instead, both models were constructed periodically with two identical interfaces.

Since silicon nitride is usually deposited onto a silicon substrate, the in-plane cell parameter of silicon nitride was adjusted to that of silicon. The middle-of-the-slab (bulk) silicon positions were locked during optimization of the positions. The slab thickness (perpendicular to the interface plane) was also relaxed. These structures were compared to relaxed structures with all degrees of freedoms unlocked (including cell dimensions and angles) and we observed a slight but insignificant increase of the binding energy and a slight change in the distance between the atomic layers close to the interfaces compared to the bulk. Furthermore, the unit cell angles did not change significantly.

The interface energy of the optimized Zhao and Bachlechner model was calculated to be 18% higher than that of the optimized interface proposed by Yang *et al.* (calculated in this study to be 1.41 J/m²). Considering this substantial difference, we thus only focus on the latter model in the rest of this work. The Si in-plane lattice constants were adopted and kept fixed in the rest of this work (this also corresponds to the real, experimental situation).

B. Bond-saturated interface model

In Fig. 1 the interface structure before and after relaxation is compared. The naming scheme, $nA(B)$, where n is the number of species A , while B an optional parameter signifying on which side of the interface the atoms reside is listed in Table I. Bond lengths for the relaxed structure are listed in Table II.

Upon relaxation of the structure, there are significant changes. The 3Si(Si)-1N distances are contracted to yield a more reasonable Si-N bond length that is only 2–3% longer than in bulk Si₃N₄. Furthermore, the 3Si(Si)-3Si(Si₃N₄) bond lengths are more similar to that of bulk silicon, although still 3% longer. This is also the case for the 1Si-3Si(Si₃N₄) bond lengths. From Figs. 1(e) and 1(f) it is also clear that it is favorable for the 1Si-3Si(Si₃N₄) and the 3Si(Si) atoms to rotate slightly out of the hexagonal Si(111) alignment. No particular distortions compared to bulk throughout the core silicon or silicon nitride parts of the model were detected. All in all, this has to be considered as a very good fit between the Si(111) and β -Si₃N₄ interface.

In order to continue our investigation of the electronic structure, the valence band offsets and the band gap were checked for convergence for different thicknesses of the silicon and silicon-nitride layers. These results are summarized in Table III. It is clear that model III (also depicted in Fig. 1) is sufficiently large to obtain reasonable convergence and was thus chosen as the base for the rest of this work, unless otherwise specified.

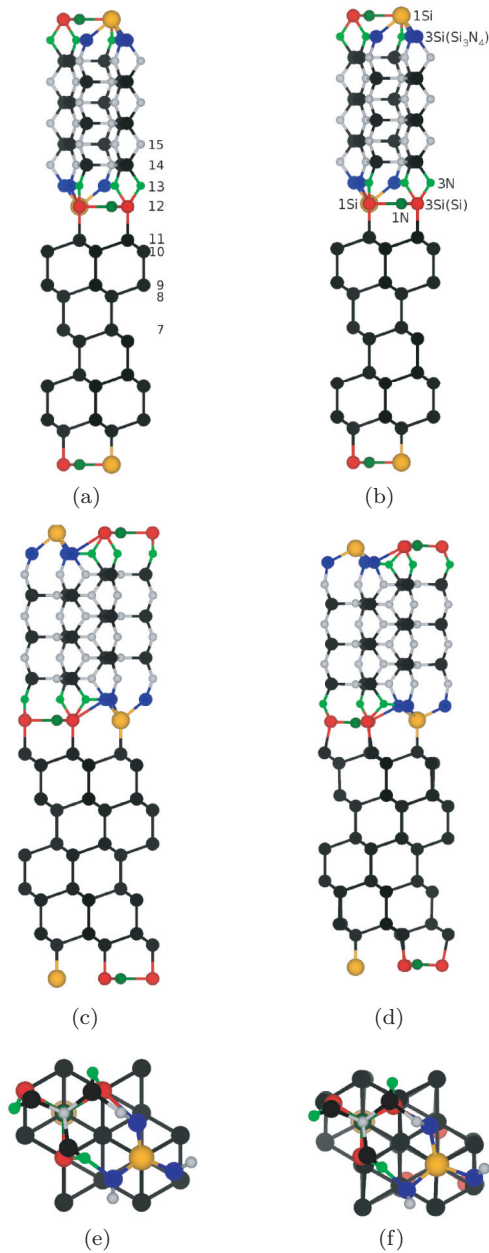


FIG. 1. (Color online) The dangling bond free interface model proposed in Ref. 9. (a) and (b) are projected along the 100 axis, (c) and (d) along the (110) axis, and (e) and (f) along the (001) axis. Left and right panels are the input and relaxed structures, respectively. See Table II for bond lengths. Naming convention used in the paper is summarized in Table I.

To qualitatively investigate the transfer of electrons close to and at the interfaces, we calculated the electron density difference maps by subtracting the superposition of overlapping free atomic electron densities from the calculated interface electron density. The result is shown in Fig. 2. The bulk Si covalent bonds are clearly illustrated as electron accumulation between the Si atoms, and the charge transfer into the sp^2 hybrid orbitals of N is also clearly visible. Furthermore, there is an electron accumulation similar to the bulk Si-Si and Si-N bonds at the interface. The similarities between the bulk semiconducting silicon and the interface bonds is clearly

TABLE I. Color scheme used for the interface atoms. See Fig. 1 for illustration.

Index	Color	Layer	Bonds to
1Si	Orange	12	3Si(Si ₃ N ₄)
3Si(Si)	Red	12	3N + 1N
3Si(Si ₃ N ₄)	Blue	13	1Si
1N	Dark green	12	3Si(Si)
3N	Light green	13	3Si(Si)

illustrated and underlines the favorable geometries compared to previous models.

Furthermore, to quantify the electronic density associated with each atom we performed a partitioning of the density using Bader’s scheme.²⁰ The results are summarized in Table IV and follow the qualitative expectations from the electron density difference plots. In the homopolar bulk Si, each Si atom is, in fact, associated with four valence electrons, while in bulk silicon nitride, nitrogen draws electrons from silicon. The nitrogen Bader occupations are all very close to the bulk Si₃N₄ value of 2.23, whereas the Si charge gradually changes from zero in bulk Si to -3.0 in Si₃N₄ (-1.39 and -0.13 at the Si side of the interface, and -1.48 at the Si₃N₄ side). Comparing the Bader occupation between the bulk and interface, there is an electron depletion from bulk Si to the interface. This transition region is expected from the electronegativity differences and occurs gradually [compare 1Si, 3Si(Si) and 3Si(Si₃N₄) to bulk Si] until bulk Bader occupation is reached.

The electronic density of states (DOS) of the interface model is given in Fig. 3, which clearly reveals its semiconducting behavior with a PBE band gap of 0.63 eV, similar to bulk silicon. The interface states are visible in the upper valence band as sharp peaks compared to the bulk states and consist mainly of 3N followed by 1Si, 3Si(Si) and 3Si(Si₃N₄) states. In the previous study⁹ these defect states were not detected. The remaining 1N states do not contribute significantly close to the band onset, but are strongly present at -1.35 to -1.20 eV. The lower conduction band is mainly dominated by 3Si(Si), 3Si(Si₃N₄), and 3N states.

To identify the interface states, we plot the projected band structure of the interface model in Fig. 4. Projection of the states onto bulk silicon, bulk silicon nitride, and interface atoms was performed. The two topmost valence bands are localized at the interface and disperse downwards from the M point. Furthermore, two additional interface states 0.8 eV below the Fermi level are visible at the M point. These states are in an energy and k -point range where corresponding bulklike Si

TABLE II. Bond lengths in the relaxed model. See Table I and Fig. 1 for details on the naming convention.

	Bond length (Å)
Bulk Si-N	1.75
Bulk Si-Si	2.36
1Si-3Si(Si ₃ N ₄)	2.29
3Si(Si)-3N	1.78
3Si(Si)-1N	1.80
3Si(Si)-3Si(Si ₃ N ₄)	2.44

TABLE III. Convergence as a function the silicon and silicon-nitride layers nL . $n\text{Si}$ and $n\text{Si}_3\text{N}_4$ indicate the number Si atom (Si bulk part) and the total number of Si_3N_4 atoms, respectively, in the interface model. Valence band offsets (VBO), and band gaps (E_g) are included. The valence band offset was calculated by aligning the core levels (see text).

	$nL/n\text{Si}$	$nL/n\text{Si}_3\text{N}_4$	d [nm]	VBO [eV]	E_g [eV]
I	6/24	6/42	1.838	0.80	0.89
II	6/24	8/56	2.131	0.88	0.82
III	12/48	8/56	3.075	0.92	0.63
IV	12/48	12/84	3.656	0.92	0.61
V	12/48	16/112	4.269	0.91	0.63
VI	12/48	20/140	4.828	0.92	0.65
VII	18/72	20/140	5.731	0.92	0.63

states are not present. Analysis of the partial band decomposed charge density in Fig. 2(b) shows that these states mostly consist of the N $2p$ orbitals oriented orthogonal to the N-Si₃ plane (the lone pair state in Si₃N₄) and bonding Si sp^3 hybrid orbitals (density accumulation between bonds and on the 1Si atom). Since the slab is symmetric with two interfaces, the states come in pairs, interacting slightly through the slab, in particular, when they approach the Γ point where bulk Si states are available to mediate the interaction through the slab. This is also clear from Figs. 2(b) and 4. However, this interaction is considered small in the context of the rest of the investigations performed in this work.

From Table III the valence band offset is 0.92 eV and significantly lower than the reported value of 1.52 eV in the previous study.⁹ It is difficult to state the exact reason without knowing details of the calculated structure and technical aspects of the previous calculation. We believe our present band offsets to be technically—within the limits of DFT—accurate to within at least 0.02 eV as demonstrated by our careful convergence tests in Table III.

An interesting aspect in the context of band alignment discussions is the interface dipole, and in particular, how much it contributes to the total band offset. In order to estimate this, we use the flat-band voltage, defined as

$$V_{\text{fb}} = \phi + \phi_d = \phi + \frac{Qd}{\epsilon A}, \quad (5)$$

where ϕ is the work function difference (macroscopic property), Q the dipole charge at the interfaces (negative for electrons), d the distance between the charged layers, ϵ the average dielectric function, and A the interface area. The second term in Eq. (5) originates from the charge difference at the interface and it modifies the flat band voltage accordingly.

In order to estimate the size of ϕ_d we need to determine Q . The electron charge transfer Q at the interface was determined by summing the Bader occupations in each atomic layer and subtracting the nominal valence occupation in the respective layer. The result is plotted in Fig. 5. We note that the line becomes essentially zero in the bulk Si and the Si₃N₄ part, since bulk Si is homopolar, and each Si₃N₄ plane consists of an almost coplanar layer of 3 Si and 4 N atoms, resulting in zero net charge for each layer. Clearly, the silicon interface atoms [layer 12 with the atoms 3Si(Si), 1Si and one 1N]

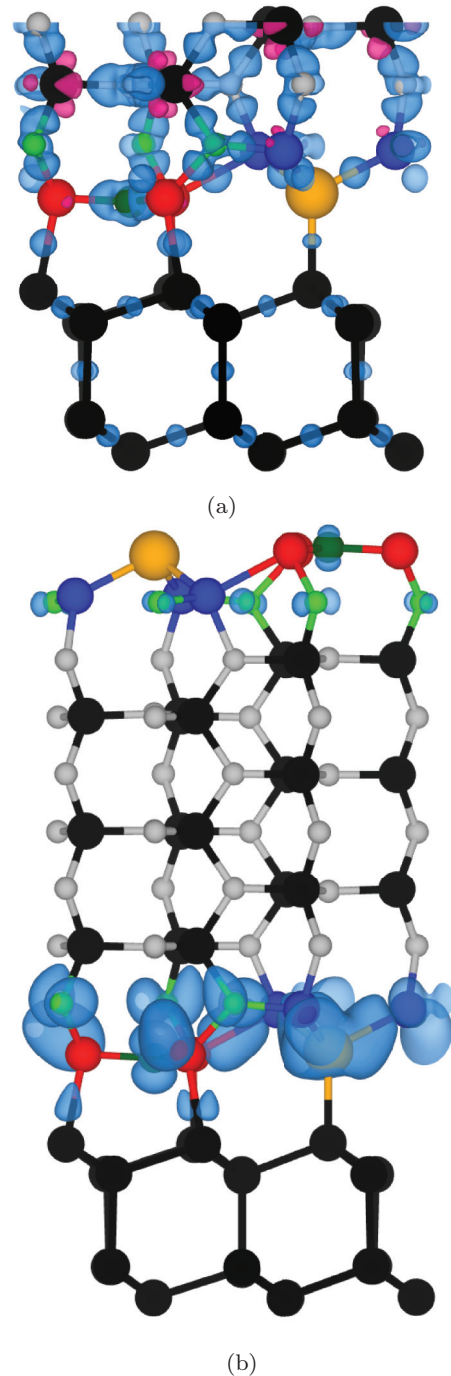


FIG. 2. (Color online) (a) Electron density difference map (self-consistent density minus atomic charge density) for the interface. Blue highlights electron accumulation, while red represents electron depletion. The isosurface level is set at 0.02 bohr^{-3} for both the negative and positive isosurfaces. (b) Electron density of one of the interface states, isosurface level at 0.002 bohr^{-3} . Residue of a small interaction between the interfaces can be seen. See Table I and Fig. 1 for details on the coloring scheme.

transfer electrons to the interface silicon-nitride layer [layer 13 with the atoms 3Si(Si₃N₄) and 3N], such that there is an electron accumulation in layer 13 and a depletion in layer 12 (see Fig. 1 for the description of the layers). This can be

TABLE IV. Bader electron density partitioning for the bulk and interface atoms. Electron transfer is calculated with respect to the free valence, also listed.

	Valence	Bader	Difference
Bulk Si(Si)	4.00	4.00	0.00
Bulk Si(Si ₃ N ₄)	4.00	1.00	-3.00
Bulk N	5.00	7.23	2.23
1Si	4.00	3.87	-0.13
3Si(Si)	4.00	2.61	-1.39
3Si(Si ₃ N ₄)	4.00	2.52	-1.48
1N	5.00	7.27	2.27
3N	5.00	7.21	2.21

explained from the difference in effective electronegativity between the two bulk constituents. Since silicon-nitride has a larger electronegativity than silicon, a positively charged layer is expected on the silicon side of the interface and vice versa. From a microscopic viewpoint, the three interfacial 3Si(Si) atoms in layer 12 donate charge to their three nearest-neighbor 3N atoms in layer 13. The migration of one N atom from layer 13 substantially helps to reduce the interface dipole, which relates to the greater stability of the model of Yang *et al.*

The net electron transfer creates an interface dipole pointing towards the silicon slab and raises the Si₃N₄ valence band compared to the Si valence band.

From Fig. 5 the average transferred charge Q is 2.29 e/layer. Assuming an average relative dielectric constant of 9.59, a surface area of 59 Å², and an interlayer distance of 1.15 Å we obtain $\phi_d = -0.84$ eV (raising the Si₃N₄ valence band), which is a significant contribution and can not be disregarded in the calculation of the flat-band voltage. To avoid any confusion, we stress that these contributions are already fully and automatically accounted for in the *ab initio* calculations and values reported in Table III.

The band offsets for the interface are illustrated in Fig. 6, including accurate QP corrections determined using the *GW* method. For the valence band and conduction band offsets, we added the corresponding *GW*₀ corrections determined previously for bulk Si and Si₃N₄ (see Ref. 11). This increases the valence band offset by 0.36 eV from 0.92 eV to 1.28 eV,

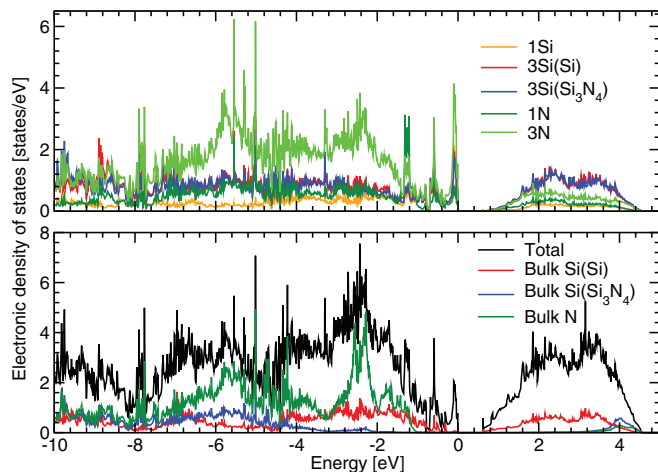
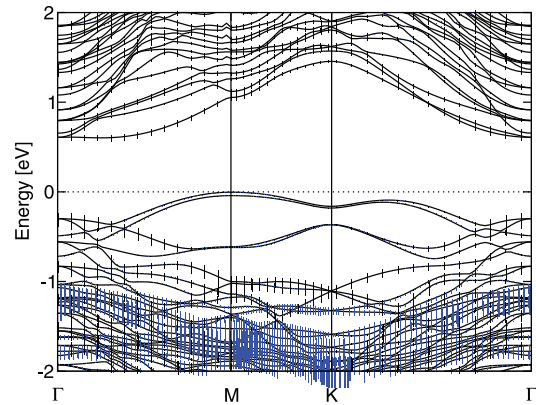
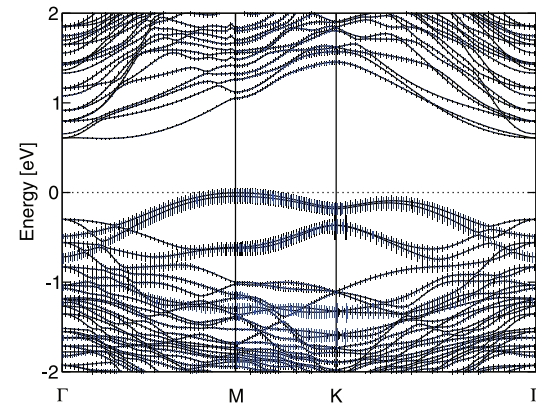


FIG. 3. (Color online) Electronic density of states for the interface (upper panel) and bulk states (lower panel).



(a) Bulk states



(b) Interface states

FIG. 4. (Color online) Projected band structure for the interface model. Top panel highlights the silicon (black bars) and silicon-nitride (blue bars) bulk states, while the bottom panel highlights the silicon (black bars) and nitrogen (blue bars) interface states (colored atoms in Fig. 1). Vertical bar size indicates the strength of the projection onto respective atoms.

and the conduction band offset by 1.0 eV. In our density-functional calculations, the least bound interface states are located at the M point and reside approximately 0.3 eV above the silicon valence band onset. In order to investigate this further, we performed *GW*₀ calculations on the interface model. The resulting relation between the quasiparticle energy and the DFT (Kohn-Sham) eigenvalues is illustrated in Fig. 6(b). The quasiparticle corrections are well approximated by a scissor correction, with the valence band maximum shifted down by 0.34 eV and the conduction band minimum shifted up by 0.11 eV. Since the band edges are dominated by Si states, we would expect a similar behavior in bulk Si and found this indeed confirmed in test calculations. We also found that the position of the interface state with respect to the bulk Si valence band states is well described by the DFT eigenvalue differences and hardly influenced by QP corrections. Note that the Si valence band is comparatively close to the Si₃N₄ valence band, whereas the conduction band offsets are quite large, a result of the interface dipole moment we have discussed before.

C. Substitutional phosphorus defects

In bulk silicon, there is a wealth of different defects and complexes, for example: substitutional phosphorus or

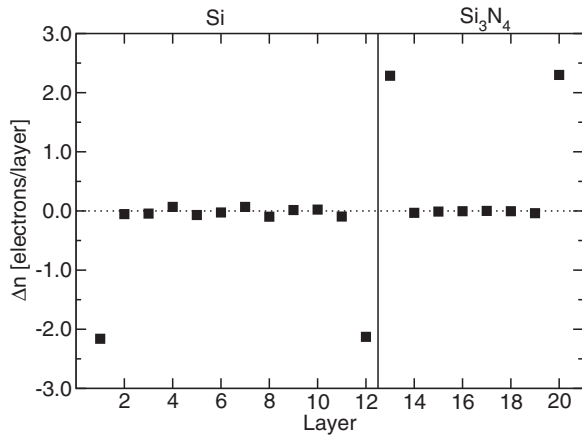


FIG. 5. Electron transfer for each atomic layer calculated by subtracting the free valence electrons from the calculated Bader electron occupancy. Vertical line indicates the interface.

boron, nitrogen monomers, nitrogen dimers, hydrogen, silicon vacancies and interstitials, and diverse complexes, some of which have yet to be discovered. Close to passivation interfaces, silicon is often heavily doped (sometimes in excess of 10^{20} cm^{-3})²² to create an *n*- or *p*-type emitter. It is reasonable to assume that the constituent dopants will play an important role at and close to the interfaces.

In this section, we turn to substitutional (for silicon) phosphorus,²³ which acts as an *n*-type dopant in most industrial

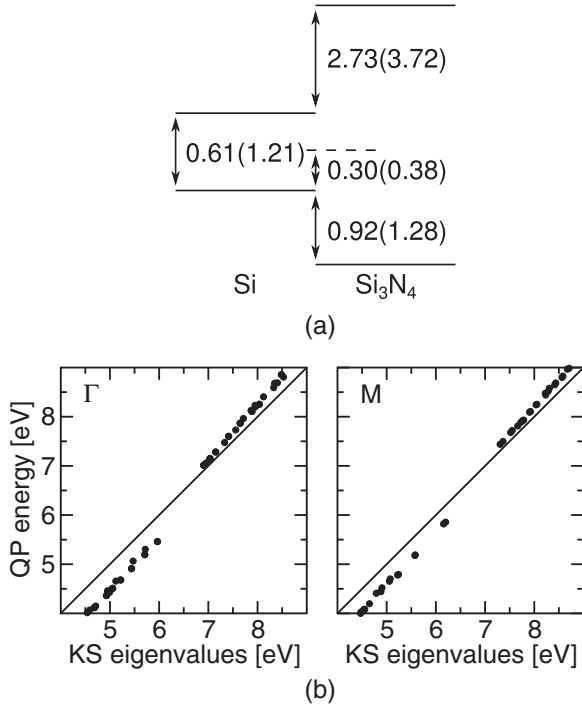


FIG. 6. (a) Band offsets from GGA-PBE (GW_0) calculations of the interface between silicon and β - Si_3N_4 . The energy levels of the M-point interface state is indicated by the dashed line. Consult Fig. 4 for additional details. (b) Comparison between the quasiparticle (QP) energies from GW_0 calculations and Kohn-Sham (KS) eigenvalues (GGA-PBE) at the Γ point (left panel) and the M point (right panel). The occupied states are located below 6.5 eV.

grade Si solar cells, and we investigate how it modifies the interface properties studied in the previous section. Another important class of defects is nitrogen, which is isovalent with phosphorus and might be incorporated in Si during the nitridation. A detailed study of nitrogen incorporation into the silicon side of the interface model is left for future studies. Furthermore, we did not consider phosphorus substituted for nitrogen in silicon nitride.

The substitutional phosphorus was placed at silicon sites in the interface model covering the range from bulk silicon to bulk silicon nitride (from layer 7 to 15 according to Fig. 1). Only one defect was introduced per slab. The different defect configurations are labeled with superscripts, where the superscript signifies the layer in which the defect resides after relaxation (compare Fig. 1). If the layer offers more than one symmetry inequivalent position [for instance 1Si or 3Si(Si)] we use the previously introduced nomenclature to identify the site. In the silicon nitride, the silicon positions are symmetry equivalent in each layer. All structures were then relaxed and the electronic structure calculated in a second step. The lattice parameters were not allowed to change during the relaxation.

In Table V the relative total energies ΔE (depicted in Fig. 7) are listed for the interface model with substitutional phosphorus located at different silicon sites. After relaxation, the substitutional phosphorus remains close to the original silicon positions for all considered configurations. The change in the total energy with respect to bulk silicon (the P^7 configuration) is fairly small when phosphorus approaches the silicon nitride, except at the interface $\text{P}^{12}/1\text{Si}$ and $\text{P}^{12}/3\text{Si}(\text{Si})$. The energies for substitution in Si_3N_4 are much less favorable and migration of substitutional phosphorus into the silicon nitride therefore seems unlikely. Already at the $\text{P}^{12}/3\text{Si}(\text{Si})$ position, silicon has three nitrogen neighbors. This position is therefore fairly unstable, whereas the position $\text{P}^{12}/1\text{Si}$ is surprisingly stable. This is most likely related to the fact that layer 12 is electron deficient according to our previous analysis (compare Fig. 5). Replacing silicon by phosphorus will increase the number of electrons in this layer and thus lower the interface dipole (see later discussion).

The substitutional phosphorus is a well studied defect in bulk *n*-type silicon²³ causing a shallow donor level in Si, and it is thus interesting to investigate how the defect level behaves in the β - $\text{Si}_3\text{N}_4(0001)/\text{Si}(111)$ system, and how the phosphorus defect modifies the interface states. In order to perform this analysis we chose two representative configurations; phosphorus in layer 7 (bulk silicon) and in layer 12 ($\text{P}^{12}/1\text{Si}$). In Fig. 8 we show the band structures and highlight the states localized on the phosphorus atom. When phosphorus resides in bulk silicon the induced defect band is located in the gap about 0.3 eV below the Si conduction band in agreement with a previous study.²³ The small lateral distance between the P atoms places the defect level at too low energies. The electron density of the phosphorus defect state in bulk silicon is illustrated in Fig. 9(a). The defect state is delocalized in the layer where P resides, but extends only a little to the neighboring layers.

Few changes in the band structure are observed when phosphorus is moved closer to the interface, however, the situation changes drastically when P resides at the interface. The conducting states (here, the range between the conduction

TABLE V. The relative total energy ΔE and $\Delta E'$ [see Eqs. (2) and (3), respectively] for substitutional phosphorus and the valence band offset E_{VBO} as a function of phosphorus layer occupancy and cell size. ΔE specifies the relative energy compared to P substitution in a bulk Si slab with similar lateral size, whereas $\Delta E'$ specifies the relative energy compared to a common reference. For $\Delta E'$, P substitution in the largest considered supercell ($3 \times 3 \times 1$ P⁷) was considered as reference [see Eqs. (2) and (3)]. Different sites in one layer are indicated using the previously introduced nomenclature. $n \times n \times 1$ indicates that the original interface model was replicated $n \times n$ times along the interface plane.

Cell	Defect	E_{VBO} [eV]	ΔE ($\Delta E'$) [eV]
1 × 1 × 1	none	0.92	
	P ⁷	0.80	0.05 (0.29)
	P ⁸	0.86	0.08 (0.32)
	P ⁹	0.91	0.07 (0.31)
	P ¹⁰	0.93	0.06 (0.30)
	P ¹¹	1.01/1.04	0.23 (0.48)/0.08 (0.32)
	P ¹² /1Si	1.26	−0.64 (−0.39)
	P ¹² /3Si(Si)	1.20	1.22 (1.45)
	P ¹³ /3Si(Si ₃ N ₄)	1.27	1.22 (1.46)
	P ¹⁴	1.78	2.49 (2.73)
	P ¹⁵	2.11	2.64 (2.89)
2 × 2 × 1	P ⁷	0.90	0.04 (0.17)
	P ⁸	0.92	0.05 (0.19)
	P ⁹	0.92	0.06 (0.20)
	P ¹⁰	0.96	0.09 (0.23)
	P ¹¹	0.98	0.22 (0.36)
	P ¹² /1Si	1.08	−0.84 (−0.70)
	P ¹² /3Si(Si)	1.06	1.05 (1.19)
	P ¹³ /3Si(Si ₃ N ₄)	1.17	1.05 (1.19)
	P ¹⁴	1.23	2.17 (2.31)
	P ¹⁵	1.33	2.21 (2.35)
	3 × 3 × 1	P ⁷	0.93
P ⁹		0.94	0.05 (0.02)
P ¹¹		0.97	0.21 (0.19)
P ¹² /1Si		1.00	−0.88 (−0.90)
P ¹³ /3Si(Si ₃ N ₄)		1.03	1.01 (0.98)
P ¹⁴		1.03	2.11 (2.09)
P ¹⁵		1.06	2.15 (2.12)

band minimum and the Fermi level) of this configuration are illustrated in Fig. 9(b). As previously discussed, our model contains two interfaces, but we have added only one P, so that one set of interface states is expected to be unmodified. Surprisingly, when phosphorus resides at the interface, the phosphorus defect level as well as the interface states at this interface vanish, although the remaining interface states corresponding to the second interface (without P) are still clearly visible in Fig. 8(c). The underlying principle is easy to understand. With a formal ionicity of -5 , P induces a rather strong attractive potential at the substitutional site. In bulk Si, this induces a shallow defect level at the conduction band edge as discussed above. At the interface, however, the—compared to Si⁴⁻—more attractive P⁵⁻ potential moves the interface states to lower energies, so that they overlap and hybridize with the neighboring Si atoms. In fact, a residual of the interface states is still clearly visible in the projected P states, but at

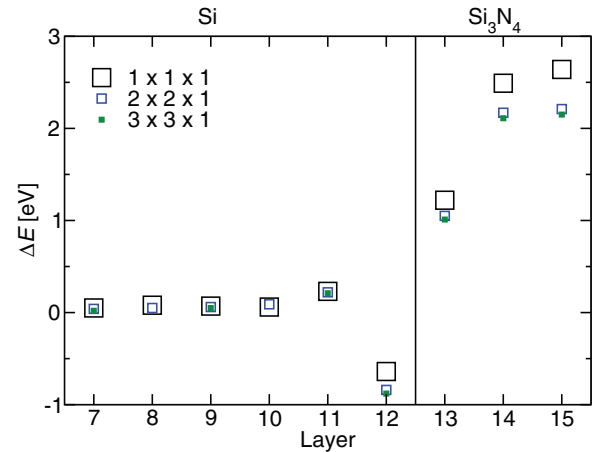


FIG. 7. (Color online) Relative total energy ΔE for three different defect concentrations for substitutional phosphorus. The layer is indicated along the vertical axis (compare Fig. 1). For all three concentrations the most stable configuration of the substitutional phosphorus is at the 1Si position. See Table V for additional details.

higher binding energies (more negative, from approximately -0.75 eV below the valence band onset down). Also note that the original interface state was partly localized on the 1Si atom (Fig. 2), where P now resides. The shallow P related donor state has also not entirely vanished, but as the interface state strongly screens the P⁵⁻ potential, it has moved up into the Si conduction band. At the *K* point it is still clearly visible but well above the bulk Si conduction bands.

We will now consider how the substitutional phosphorus changes the valence band offset. With one phosphorus embedded, this yields a phosphorus concentration of 1.02×10^{21} . The valence band offsets are presented in Table V and Fig. 10. In order to interpret these results, we investigated the electron transfer at the interface and how it is modified by the defect configurations. We again calculated the averaged Bader electron occupations, similar to Fig. 5. The results are depicted in Fig. 11 and reveal changes to the charge in the slabs and at the interface. We note that, since we have subtracted the formal ionic charges of P and Si from the Bader charges, $\Delta n = 0$ corresponds to a layer which is formally charge neutral. When phosphorus is introduced in silicon there is a sizable electron accumulation in the defect occupying layer. The electron surplus of $+1$ in this layer implies that in addition to the five P valence electrons, one more electron is found in this layer. This is most likely an artifact of the Bader analysis, which is not necessarily unerring for covalent materials with significant charge accumulation along the bonds. Including the nearest-neighbor layers, however, restores charge neutrality around the defective layer as expected.

Silicon nitride can also not accommodate the extra electron from P in the valence band, and the additional electron needs to move into the conduction bands. Since the energetic position of the Si conduction band is below that of the Si₃N₄ (compare Fig. 6), the charge will be transferred towards the Si bulk part—the Bader analysis assigns the transfer to the interface layer 13—until an opposing dipole develops that ultimately aligns the Si₃N₄ and the Si conduction bands. This relates well to the huge increase of the valence band offset visible in Fig. 10:

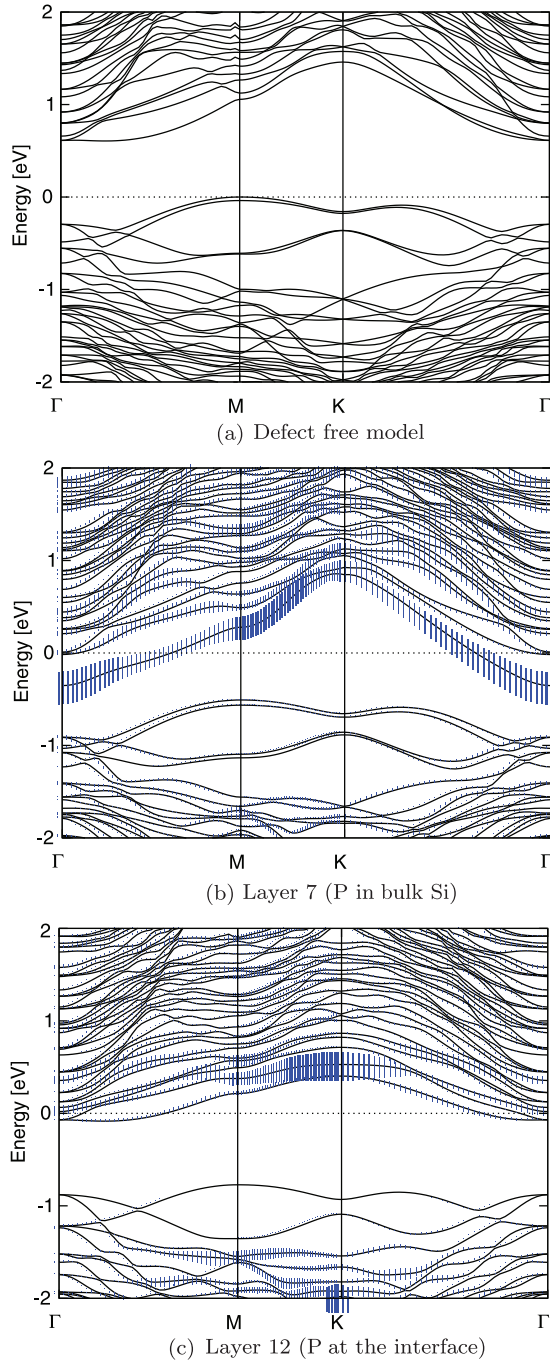


FIG. 8. (Color online) Band structure of the interface (a) without phosphorus, (b) phosphorus in layer 7 (in bulk silicon), (c) phosphorus in layer 12 (at the interface). The vertical blue bars are projected phosphorus states and their vertical size determines the strength of the localization on the P atom.

as a result of the dipole, the Si valence band shifts upwards compared to the Si_3N_4 valence band until both conduction bands are identical counteracting the charge transfer from the P defect into the Si bulk. For more elongated supercells the valence band offset might increase even further, but since P doping into Si_3N_4 is energetically so unfavorable, this is not a scenario warranting further investigations.

At the intermediate positions, in particular for P in the 1Si position, the situation is intermediate. The extra P valence

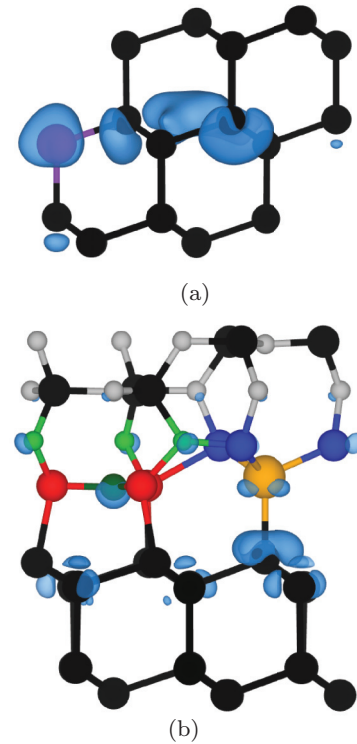


FIG. 9. (Color online) Electron densities of (a) the occupied conduction band state for a phosphorus defect (purple) state in bulk silicon (isosurface level set at 0.002 bohr^{-3}), and (b) the occupied conduction band state for phosphorus substitution (here at the orange position) at its most stable interface position (isosurface level set at 0.001 bohr^{-3}). For a color legend, see Fig. 1.

electron (compared to Si) can not be accommodated in the Si valence band. As for P in bulk Si, the additional conduction band electron will remain bound to the P ion, although the center of the electronic charge surplus will be located towards the Si side of the interface, since the Si conduction band is at much lower energies than the Si_3N_4 conduction band.

The Bader charges clearly confirm this picture with a huge increase of the charge at layer 12 and a decrease at layer 13 (compared to the reference values without P). This obviously counteracts the dipole at the silicon-nitride/silicon interface with no P defects. Essentially, phosphorus restores the natural band alignment between silicon nitride and silicon. Microscopically, we can relate this to the larger electronegativity of P than Si. At the interface without P, the electronegative N attracts charge from the neighboring Si, but when the more electronegative P instead of Si is located at the interface the charge transfer is much smaller. Using the dipole model from Eq. (5), we can even quantify the change in the valence band offset and the corresponding results are listed in Table VI. It is evident that the change in valence band offset is fully accounted for by the lowering of the interface dipole, in compliance with Fig. 11 and previous discussions.

Finally, we note that the valence band offset in Fig. 10 is slightly decreased when phosphorus resides in silicon bulk. This is mostly due to the change ($\sim 0.1 \text{ eV}$) in the reference energy used for the silicon and silicon nitride in the interface model and stems from the difference in the electrostatic potential. We believe this is an artifact of a rather small

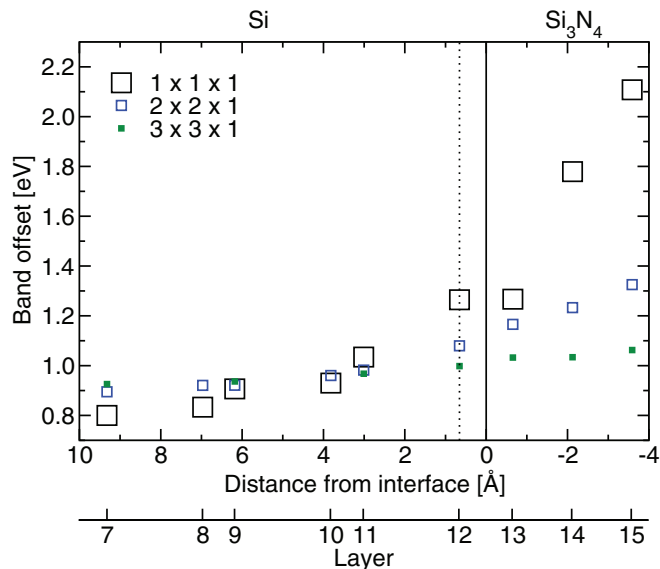


FIG. 10. (Color online) Valence band offset with phosphorus occupying the specified layers. The inset shows the distance to the surface (negative in Si₃N₄). See text for defect concentrations associated with the cell size (illustrated by the differently sized square points). Vertical solid line indicates the interface, while the vertical dotted line indicates the most stable phosphorus position.

supercell model, but it is difficult to explicitly show this due to the difficulties of constructing models of similar phosphorus concentration without phosphorus-phosphorus interaction.

The defect concentration of the previous calculations is large. Although silicon is often aggressively doped close to the interface of silicon nitride in solar cells to create the emitter and although we believe values in the 10²¹ cm⁻³ range to be representative of industrially used samples, we would like to pursue this issue further. In order to investigate this, two additional models were considered; a 2 × 2 × 1 and a 3 × 3 × 1 supercell, corresponding to phosphorus defect concentrations in silicon of 2.56 and 1.13 × 10²⁰ cm⁻³, respectively. In Fig. 7 the relative total (interface) energy is plotted as a function of the phosphorus configuration. All concentrations yield similar qualitative behavior as previously discussed; for example, the energetically most stable phosphorus configuration is still at the 1Si position and the valence band offset increases (decreases) as phosphorus is moved closer to the interface from bulk silicon (silicon nitride) (see Fig. 10). As the phosphorus concentration decreases, smaller changes of the valence band offset are observed, and the values converge towards the valence band offset of the defect free model.

TABLE VI. Correlation between the electron transfer, interface dipole energy ϕ_d , and valence band offsets for three representative configurations; the defect free interface model, phosphorus in the Si part (P⁷) and at the interface (P¹²/1Si configuration).

	Defect free	P ⁷	P ¹² /1Si
Elect. trans. [e]	2.29	2.29	0.89
ϕ_d [eV]	-0.84	-0.84	-0.33
VBO [eV]	0.92	0.8	1.26

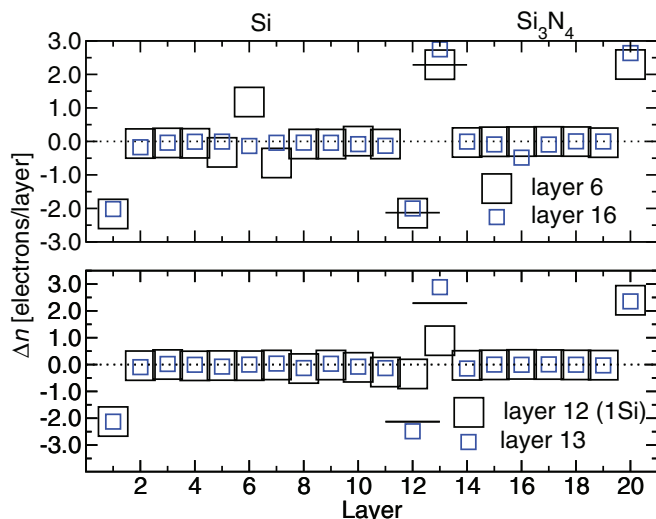


FIG. 11. (Color online) Electron transfer for each atomic layer (see Fig. 1). The electron transfer was calculated by subtracting the atomic valence (4 for Si, 5 for P) from the calculated Bader electron occupation (see text for details). The upper panel shows results for P in bulk silicon (layer 6) and silicon nitride (layer 16), while the lower panel shows results for substitution in layer 12 (most stable position) and 13 (at the interface). The short solid lines represent the bulk values from Fig. 5.

Since P substitution at the interface is energetically so stable (-0.39 eV compared to a single P atom in bulk Si in the low doping limit), it seems reasonable to assume that every 1Si atom at the interface will be substituted by a P atom corresponding to our 1 × 1 × 1 model. Adding the *GW*₀ corrections for the band alignment, we obtain a valence band offset of 1.57 eV, which is in the range of measured values (1.5 to 1.9 eV) for the band alignment of silicon nitride on silicon.^{4,6,8,13}

Although we have not repeated the *GW*₀ calculations for phosphorus substitution at the interface, we expect this result to be valid, as (i) the *GW*₀ shifts are essentially bulk Si and silicon nitride properties, and (ii) the electrostatic effects introduced by P doping are expected to be accurately accounted for by density functional theory.

IV. SUMMARY AND FINAL REMARKS

We have investigated the β -Si₃N₄(0001)/Si(111) interface by employing the recent model proposed by Yang and coworkers,⁹ studying the interface geometries, charge transfer, and band alignment in detail. The relaxed interface geometry yields fourfold coordinated silicon and threefold coordinated nitrogen atoms, similar to bulk Si and β -Si₃N₄. Although the interface atoms are consequently fully saturated, a well defined interface state is observed partly residing in the silicon gap. This defect state is related to silicon *sp*³ hybrid orbitals oriented towards the nitride and contains contributions from nitrogen lone pair states, causing a sizable charge transfer into the silicon nitride. The resulting dipole decreases the valence band offsets between silicon and silicon nitride significantly by about 0.8 eV.

The DFT band offsets were corrected by quasiparticle *GW*₀ calculations, resulting in an increase in the valence

offset from 0.92 eV (DFT) to 1.28 eV, which is still small compared to the experimental estimates of 1.5–1.9 eV—the small value of the model certainly being a result of the large interface dipole. Since industrial solar cells usually are strongly phosphorus doped, the present study also covers substitutional phosphorus in bulk silicon, silicon nitride, and at the interface. Substitutional phosphorus in silicon nitride is found to be very unfavorable and can be ruled out on energetic grounds. However, even at high concentrations at the interface, substitutional phosphorus is more stable than in low concentrations in the silicon bulk. This implies a strong phosphorous segregation towards the interface. In the particular model considered here, every fourth Si atom at the interface is substituted by phosphorus. Remarkably, at the most favorable position, phosphorus entirely removes the interface states as well as the shallow donor state related to phosphorus, relating well with the high stability of phosphorus at the interface. Furthermore, phosphorous substitution at the

interface significantly reduces the interface dipole and hence increases the valence band offset to a value around 1.6 eV (including the $G W_0$ corrections). This brings the valence band offset in good agreement with experiment.

Generally, our present results clearly demonstrate that phosphorus doping (and possibly other doping) can have a huge impact on the interface between silicon and silicon nitride. In fact, it is also experimentally observed that n doping using phosphorus changes the properties of the silicon/silicon-nitride interface significantly, for instance enhancing contact formation between metallic Ag leads and silicon. As we predict strong phosphorus segregation to the interface, this experimental observation certainly does not come as a surprise.

ACKNOWLEDGMENT

We would like to acknowledge the European Union FP7 project Hipersol for financial support and the NOTUR consortium for computational resources.

*espen.flage-larsen@sintef.no

¹F. L. Riley, *J. Am. Ceram. Soc.* **83**, 245 (2000).

²A. G. Aberle, *Sol. Energ. Mater Sol. Cells* **65**, 239 (2001).

³R. Kärcher, L. Ley, and R. L. Johnson, *Phys. Rev. B* **30**, 1896 (1984).

⁴J. W. Keister, J. E. Rowe, J. J. Kolodziej, H. Niimi, T. E. Madey, and G. Lucovsky, *J. Vac. Sci. Technol. B* **17**, 1831 (1999).

⁵S. Miyazaki, M. Narasaki, A. Suyama, M. Yamaoka, and H. Murakami, *Appl. Surf. Sci.* **216**, 252 (2003).

⁶W. M. K. V. A. Gritsenko, A. V. Shaposhnikov, H. Wong, and G. M. Jidomirov, *Thin Solid Films* **437**, 135 (2003).

⁷M. Higuchi, S. Sugawa, E. Ikenaga, J. Ushio, H. Nohira, T. Maruizumi, A. Teramoto, T. Ohmi, and T. Hattori, *Appl. Phys. Lett.* **90**, 123114 (2007).

⁸H.-L. Lee, C.-T. Kuo, H.-W. Shiu, C.-H. Chen, and S. Gwo, *Appl. Phys. Lett.* **95**, 222104 (2009).

⁹M. Yang, R. Q. Wu, W. S. Deng, L. Shen, Z. D. Sha, Y. Q. Cai, Y. P. Feng, and S. J. Wang, *J. Appl. Phys.* **105**, 024108 (2009).

¹⁰G. L. Zhao and M. E. Bachlechner, *Phys. Rev. B* **58**, 1887 (1998).

¹¹G. Kresse, M. Marsman, L. E. Hintzsche, and E. Flage-Larsen, *Phys. Rev. B* **85**, 045205 (2012).

¹²J. W. Kim and H. W. Yeom, *Phys. Rev. B* **67**, 035304 (2003).

¹³A. Iqbal, W. B. Jackson, C. C. Tsai, J. W. Allen, and C. W. B. Jr., *Appl. Phys. Lett.* **61**, 2947 (1987).

¹⁴J. P. Perdew, K. Burke, and M. Ernzerhof, *Phys. Rev. Lett.* **77**, 3865 (1996).

¹⁵G. Kresse and J. Hafner, *Phys. Rev. B* **47**, 558 (1993).

¹⁶G. Kresse and J. Hafner, *Phys. Rev. B* **49**, 14251 (1994).

¹⁷VASP code, <http://cms.mpi.univie.ac.at/vasp>

¹⁸B. R. Tuttle, *Phys. Rev. B* **67**, 155324 (2003).

¹⁹W. Tang, E. Sanville, and G. Henkelman, *J. Phys.: Condens. Matter* **21**, 084204 (2009).

²⁰R. F. W. Bader, *Atoms in Molecules: A Quantum Theory* (Oxford University Press, New York, 1990).

²¹K. Momma and F. Izumi, *J. Appl. Crystallogr.* **44**, 1272 (2011).

²²S. Peters, C. Ballif, D. Borchert, R. Schindler, W. Warta, and G. Willeke, *Semicond. Sci. Technol.* **17**, 677 (2002).

²³G. L. Pearson and J. Bardeen, *Phys. Rev.* **75**, 865 (1949).